



Dosimetry of small photon fields in the presence of bone heterogeneity using MAGIC polymer gel, Gafchromic film, and Monte Carlo simulation

Wrya Parwaie¹, Ghazale Geraily^{2,3}, Ghazal Mehri-Kakavand⁴, Somayyeh Babaloui², Samira Rezvani², Mohamad Pursamimi⁴

¹Department of Medical Physics, Faculty of Paramedical Sciences, Ilam University of Medical Sciences, Ilam, Iran

²Department of Medical Physics and Biomedical Engineering, School of Medicine, Tehran University of Medical Sciences, Tehran, Iran

³Cancer Institute, Imam Khomeini Hospital, Tehran University of Medical Sciences, Tehran, Iran

⁴Department of Medical Physics, School of Medicine, Semnan University of Medical Sciences, Semnan, Iran

ABSTRACT

Background: The presence of heterogeneity within the radiation field increases the challenges of small field dosimetry. In this study, the performance of MAGIC polymer gel was evaluated in the dosimetry of small fields beyond bone heterogeneity.

Materials and methods: Circular field sizes of 5, 10, 20 and 30 mm were used and Polytetrafluoroethylene with density of 2.2 g/cm³ was used as the bone equivalent material. The PDD curves, beam profiles, and penumbra widths were measured using MAGIC polymer gel, EBT2 film, and Monte Carlo simulation.

Results: The maximum differences between MAGIC and EBT2 are 6.1, 4.7, 2.4, and 2.2 for PDD curves at 5, 10, 20, and 30 mm circular fields, respectively. The dose differences and distance to agreement between MAGIC and MC were within 1.89%/0.46 mm, 1.66%/0.43 mm, 1.28%/0.77 mm, and 1.31%/0.81 mm for beam profile values behind bone heterogeneity at 5, 10, 20, and 30 mm field sizes, respectively.

Conclusion: The results presented that the MAGIC polymer gel dosimeter is a proper instrument for dosimetry beyond high density heterogeneity.

Key words: small field; bone heterogeneity; MAGIC polymer gel; Monte Carlo simulation

Rep Pract Oncol Radiother 2022;27(2):226-234

Introduction

With the advent of modern radiotherapy techniques such as intensity modulated radiotherapy (IMRT), volumetric modulated arc radiotherapy (VMAT), stereotactic radiosurgery (SRS), and stereotactic body radiation therapy (SBRT), the importance of the dosimetry in small photon fields has increased day by day [1]. The accuracy of dose delivered to the target volumes and healthy organs is highly dependent

on the accuracy of entering data to the treatment planning system (TPS) to determine the dose inside the radiation field. These data include output factors (OFs), off axis ratio (OARs), and percentage depth doses (PDDs) [2]. More accuracy in dose calculation and dose delivery led to improvement of tumor control probability, decrease normal tissue toxicity and therefore better treatment outcomes [3].

In the small field dosimetry, there are several complicated issues that make this type of dosimetry

Address for correspondence: Ghazale Geraily, Medical Physics Department, Tehran University of Medical Science, Tehran, Iran, Iran Gamma Knife Center, Tehran, Iran, tel: +989124308726; e-mail: gh-geraily@sina.tums.ac.ir

This article is available in open access under Creative Common Attribution-Non-Commercial-No Derivatives 4.0 International (CC BY-NC-ND 4.0) license, allowing to download articles and share them with others as long as they credit the authors and the publisher, but without permission to change them in any way or use them commercially

a challenging subject. Some of these issues are the steep gradient of radiation dose, lateral electronic disequilibrium (LED), partial occlusion of radiation source, beam alignment, and inability to use reference dosimeter [3]. Furthermore, in presence of heterogeneous media like bone and lung, more considerations are necessary because of the beam perturbation [4].

Generally, for avoiding the challenges related to the small field dosimetry, an appropriate dosimeter should be used with some specifications such as high spatial and dose resolution, radiological tissue equivalent, and energy, dose rate, and direction independence [4–6].

Previous studies have investigated the validation of several dosimeters to acquire the dose distribution in small fields [7, 8]. Each detector has some advantages despite its drawbacks. For instance, the ionization chamber is a large size detector and so inappropriate in the steep dose gradient region [9]. Diodes readout is dependent on beam direction and MOSFET is angular dependent. Also, both of them can perturbed beam distribution [3].

although there are no recognized reference dosimeters for small field dosimetry; polymer gels have promising properties, such as high spatial resolution, energy and direction independence, 3D dose distribution measurement, and soft tissue equivalency. however it should be noted that fabrication and reproducing of gel dosimeters is difficult and highly dependent on oxygen presence in producing procedure [10]. Polymer gel dosimeters could be appropriated tools to measure the 3D dose distribution and relative beam parameters such as PDD and beam profile in small fields especially in the presence of heterogenic medium [11–14]. This type of dosimeter was used in several studies to determine its efficiency in small field dosimetry [15–19].

MAGIC (Methacrylic and Ascorbic acid in Gelatin Initiated by Copper) polymer gels are known as a normoxic gel that consists of methacrylic acid as a monomer, ascorbic acid as an antioxidant, and gelatine as gel matrix [20]. Each polymer gel dosimeter has specific properties that individuate it from other gel dosimeters. On the other hand, to date, the ability of MAGIC to obtain dose distributions in small field's photon at the presence of bone inhomogeneity has not been investigated. Therefore, the purpose of this project was to evaluate the efficacy

of MAGIC polymer gel in the measurement of dosimetric parameters beyond bone inhomogeneity in small irradiation fields. In addition, the Monte Carlo simulation as an accurate dose calculator in complex conditions such as the presence of inhomogeneity in small photon fields and EBT2 Gafchromic film as an experimental dosimeter were used to compare the data obtained by MAGIC gel dosimeter.

Materials and methods

Gel preparation

In this study, we used a MAGIC polymer gel dosimeter in order to measure the small field's dose distribution. The MAGIC was produced based on Fong [20] method and prepared under normoxic (atmospheric) conditions. The components of the MAGIC were: gelatin (swine skin, 300 Bloom, Sigma Aldrich company), hydroquinone (Sigma Aldrich company), copper sulfate (pentahydrate, 98%, Sigma Aldrich company), methacrylic acid (purity grade approximately 99%, Merk company), ascorbic acid (minimum 99%, Sigma Aldrich company), and deionized water. Firstly, water and gelatin were located in a flask, it takes about 15 minutes to soak the gelatin; the solution was heated to about 50°C. The stirring was continued at this temperature until the complete dissolution of gelatin in water. Then the heater turned off and hydroquinone added to the mixture. The ascorbic acid, methacrylic acid, and copper sulfate were added to the solution when the mixture's temperature decreased to 37°C. The gel filled in the phantoms and calibration vials, and sealed by parafilm to prevent further contact with air. Finally, the vials and phantoms kept in the refrigerator at 4°C for two days.

Phantoms

Four phantoms made of Plexiglas sheets with the dimension of $3 \times 3 \times 16$, $3 \times 3 \times 16$, $4 \times 4 \times 16$ and $6 \times 6 \times 16$ cm³ were used for circular fields with diameter of 5, 10, 20, and 30 mm, respectively. The thickness of the Plexiglas sheets was 2 mm. Also, the vials with size of 15mm diameter and 100 mm length were used to obtain the gel calibration curve. All vials filled by MAGIC gel dosimeter and sealed by screw caps and parafilm to prevent oxygen and impurities penetration. The above-mentioned phantoms were utilized to measure the beam profiles in the homogeneity situation. Polytetraflu-

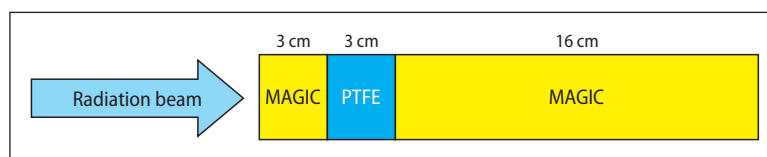


Figure 1. Schematic view of the experimental setup for MAGIC gel dosimetry in the presence of bone equivalent heterogeneity. MAGIC — methacrylic and ascorbic acid in gelatin initiated by copper; PTFE — polytetrafluoroethylene

oroethylene (PTFE) with density of 2.2 g/cm^3 was used as the bone equivalent material (high-density heterogeneity) [21]. To obtain the PDD and profile curves in the presence of high-density heterogeneity, the phantoms were located under 3cm MAGIC gel dosimeter and 3 cm bone heterogeneity as shown in Figure 1.

Gel irradiation

The irradiation of gel phantoms was conducted by Varian 2100C/D linear accelerator two days after gel preparing. To achieving the circular field sizes, the linear accelerator was equipped with home-made radiosurgical collimator including four divergent cylindrical cones and a collimator holder. The collimator cones are made of cadmium-free cerrobend alloy. This alloy was melted and poured into the steel cylinders in order to achieve cylinder shaping. Then, an isocentric hole was created in each cylinder, separately. The diameters of the holes were 5, 10, 20, and 30 mm. The collimator cones are connected to the linear accelerator head via a holder. The holder is a metal plate that was inserted into the wedge mount of the gantry. To produce a circular field sizes, the cone collimator is screwed to the holder, as shown in Figure 2.



Figure 2. A photograph of four conical collimators and a collimator holder used in the present work

The irradiation conditions were determined as follows: photon energy = 6 MV, dose rate = 400 cGy/min, source to surface distance (SSD) = 100 cm and, circular field's size = 5, 10, 20, and 30 mm. For characterizing the PDD and profile curves, all phantoms received a dose of 8 Gy at a depth of 1.5 cm. To deliver the determined dose to phantoms using each cone collimator, the monitor units were obtained using MP3 Water Phantom (PTW, Freiburg, Germany) and pinpoint ion chamber (type 31014, PTW, Freiburg, Germany) based on Protocol No. 483 [22].

For gel calibration, the calibration vials were placed in a big phantom with full scattering conditions (with dimensions of $30 \times 30 \times 30 \text{ cm}^3$) as perpendicular to the beam direction. One of the vials was not irradiated and was considered as the control vial. The others vials were irradiated by different doses of 1, 2, 3, 4, 5, 6, 8 and 10 Gy at $30 \times 30 \text{ cm}^2$ field size, SSD of 100 cm and depth of 5 cm.

MRI gel scanning

After two days from gel irradiation, the MRI scanning was done by a 3T Siemens MRI scanner. 12 hours before the scanning, phantoms and vials were placed in the MRI scanning room in order to eliminate errors in the signal's determination caused by temperature changes. Calibration vials and phantoms were scanned together to elude deviations. Imaging parameters were selected as follows: number of echo = 32, initial echo time = 14 ms, steps of echo time = 14 ms, the repetition time (TR) = 3000 ms, field of view (FOV) = $180 \text{ mm} \times 180 \text{ mm}$, matrix size 384×384 pixels. To achieve high signal-to-noise ratio (SNR) and resolution images, number of acquisitions (NEX) and slice thickness were selected 4 and 2 mm, respectively. Spin lattice relaxation rate (R_2) maps were extracted by MATLAB (The Math Works, Inc., and Natick, Massachusetts, USA) software. In order to evaluate the uncertainty measurement, all measurements are performed in triplicate.

EBT2 film dosimetry

Gafchromic EBT2 films (International Specialty Products; Ashland Inc) were used in this study to compare with gel dosimetry data in the same condition. For PDD acquisition, films were oriented in a parallel direction with the beam axis; also beam profiles were measured in a perpendicular direction with the beam axis at depth of 10 cm. A single dose of 200 cGy was delivered to all films at a depth of 1.5 cm with SSD of 100 cm. For film calibration, the pieces of films with a size of $3 \times 3 \text{ cm}^2$ were located in solid water slabs. The films were exposed by doses of 25 to 300 cGy in 25 cGy steps at the SSD = 100 cm, field size = $10 \times 10 \text{ cm}^2$, and depth = 5 cm. A piece of films was not irradiated and was considered as the control.

A day after irradiation the films were scanned with a MICROTEK 9800 XL (Microtek International Inc, USA). To reduction of the warming-up effect on scanned data, the scanner was turned on 30 minutes before scanning. All film pieces were placed at the center of the scanner and then scanned in 48-bit RGB color mode and 150 dpi resolutions. The uncompressed tagged image file format (TIFF) was selected for all images. Image J software was used to analyze the film's data and the doses were acquired in the red channel due to the highest response in the red color channel [23]. All measurements are done in triplicate in order to estimate the uncertainty measurement.

Monte Carlo simulation

The radiation transport through the accelerator treatment head was simulated by the BEAMnrc and DOSXYZnrc user codes of EGSnrc in this research. For validation of the simulation, obtained data from simulation were compared with ion chamber measurements for field sizes $3 \times 3 \text{ cm}^2$ to $10 \times 10 \text{ cm}^2$. The photon cutoff energies (PCUT) and electron cutoff energies (ECUT) were defined 0.01 MeV and 0.512 MeV, respectively. Global electron cutoff (ESAVE) was used 2 MeV for all modules except the target. The directional bremsstrahlung splitting (DBS) technique was employed with a bremsstrahlung splitting number (NBRSP) = 1000.

To achieve the statistical uncertainty below 0.5%, the number of initial particles was added and adjusted for each field size. Also, a $50 \times 50 \times 50 \text{ cm}^3$ water phantom defined in the DOSXYZnrc code. For considering of OARs and PDDs, the voxel di-

mensions were determined $0.05 \times 0.05 \times 0.2 \text{ cm}^3$ and $0.2 \times 0.2 \times 0.2 \text{ cm}^3$, respectively. For comparison between measured and calculated data, the dose differences (DD) and distance to agreement (DTA) were applied in low dose gradient area and high dose gradient area, respectively.

Results

MAGIC polymer gel and Gafchromic film calibration curves

In Figure 3, the value of R_2 versus the absorbed dose was obtained for gel dosimeter calibration vials. MATLAB was used for regression analysis. The slope and linear correlation coefficient of the calibration curve was calculated for doses from 0 to 10 Gy and the values of 0.815 ± 0.04 and 0.995 were obtained for them, respectively. In addition, optical density against absorbed dose was acquired for EBT2 film dosimeter. The results are shown as a curve in Figure 4. In order to make the EBT2 calibration curve, the measured values were matched with the second polynomial equation. As a result, the linear correlation coefficient of the film calibration curve was 0.999.

Percentage depth doses

The measured depth doses with MAGIC gel and EBT2 films and calculated with MC in heterogeneous phantom are shown in Figure 5. All the percentage depth dose values were normalized to the maximum dose and then the maximum difference between them in behind of the buildup area was determined. For PDD values behind the bone heterogeneity, the maximum differences be-

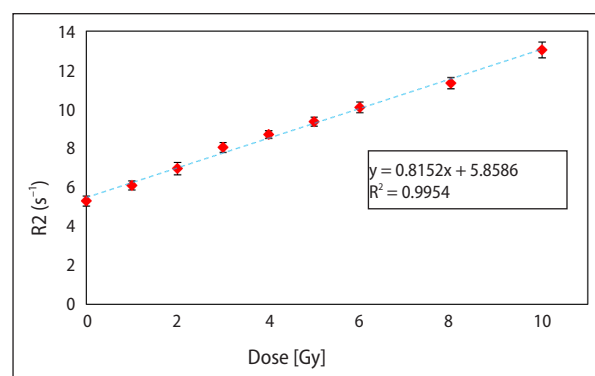


Figure 3. Dose-response of MAGIC polymer gel dosimeter in the dose range 0–10 Gy

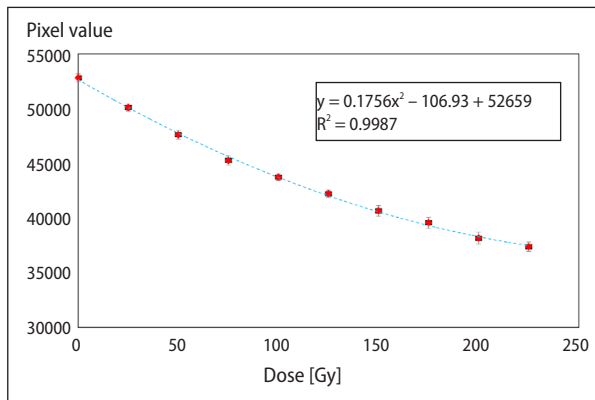


Figure 4. Pixel value versus absorbed dose for the EBT2 film Gafchromic

tween MAGIC gel dosimeter and EBT2 film are $6.1 \pm 0.3\%$, $4.7 \pm 0.4\%$, $2.4 \pm 0.2\%$, and $2.2 \pm 0.2\%$, for the 5, 10, 20, and 30 mm circular fields, respectively. Also, behind the bone heterogeneity, the maximum differences between MAGIC gel dosimeters and MC calculations are $4.2 \pm 0.2\%$, $2.5 \pm 0.3\%$, $2.1 \pm 0.4\%$, and $1.3 \pm 0.2\%$, for the aforementioned fields, respectively. Furthermore, these differences between EBT2 films and MC calculations are obtained $5.6 \pm 0.4\%$, $3.9 \pm 0.2\%$, $2.8 \pm 0.3\%$, and

$2.4 \pm 0.3\%$ for the 5, 10, 20, and 30 mm circular fields, respectively.

Off axis ratio

The off-axis dose profiles measured with MAGIC gel and EBT2 and calculated with MC for 5, 10, 20, and 30 mm diameter field sizes at 10 cm depth are shown in Figure 6. To normalize the beam profiles, all measured data were divided to the central axis value for each separate beam. Because the profiles are symmetrical for all field sizes, only half of the profiles are displayed for better clarity. The DD and DTA between MAGIC measurements and MC calculation were within 1.89%/0.46 mm, 1.66%/0.43 mm, 1.28%/0.77 mm, and 1.31%/0.81 mm for field sizes of 5, 10, 20, and 30 mm, respectively.

In the next step, The penumbra widths (80–20%) and (90–10%) were measured with MAGIC, EBT2 film in behind the heterogeneous medium at 10 cm depth for 5, 10, 20, and 30 mm diameter field sizes. Then, these data were compared with MC calculated penumbra. The results are shown in Table 1. In addition, penumbra widths (80–20%) and (90–10%) were calculated by MC at the depth of 10 cm in the homogeneity phantom for field sizes of

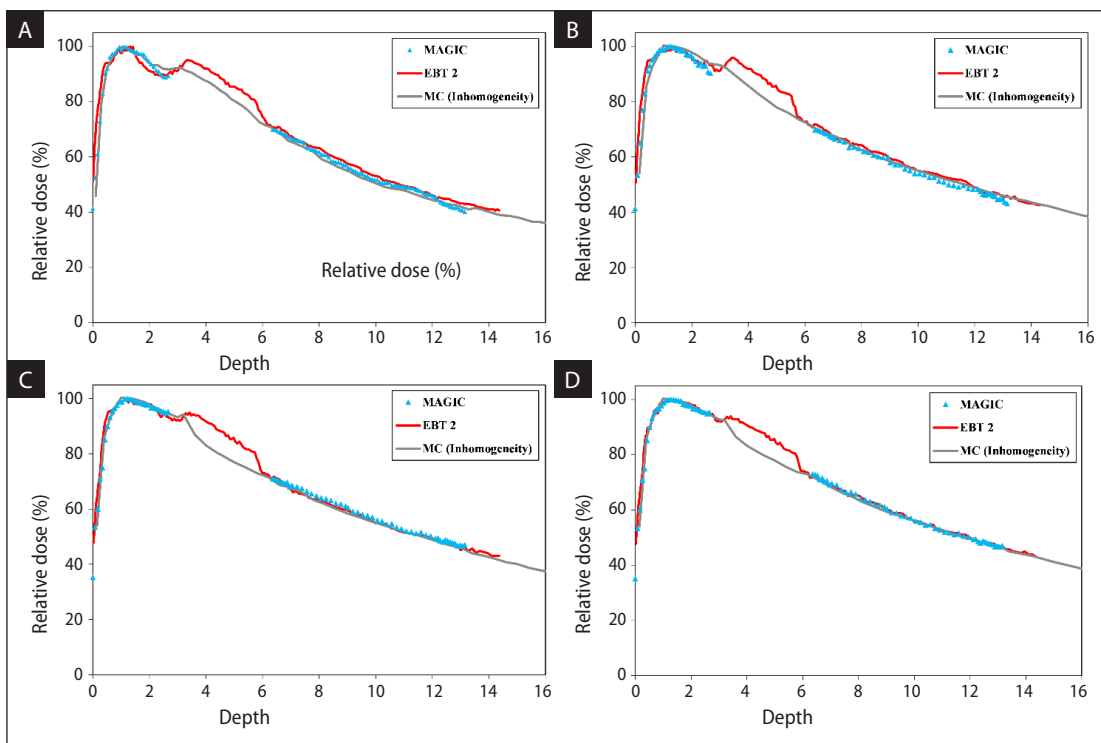


Figure 5. Percentage depth dose curves in the presence of bone heterogeneity using the EBT2 film, MAGIC, and Monte Carlo calculations for 5 mm (A); 10 mm (B); 20 mm (C), and 30 mm (D) circular field sizes

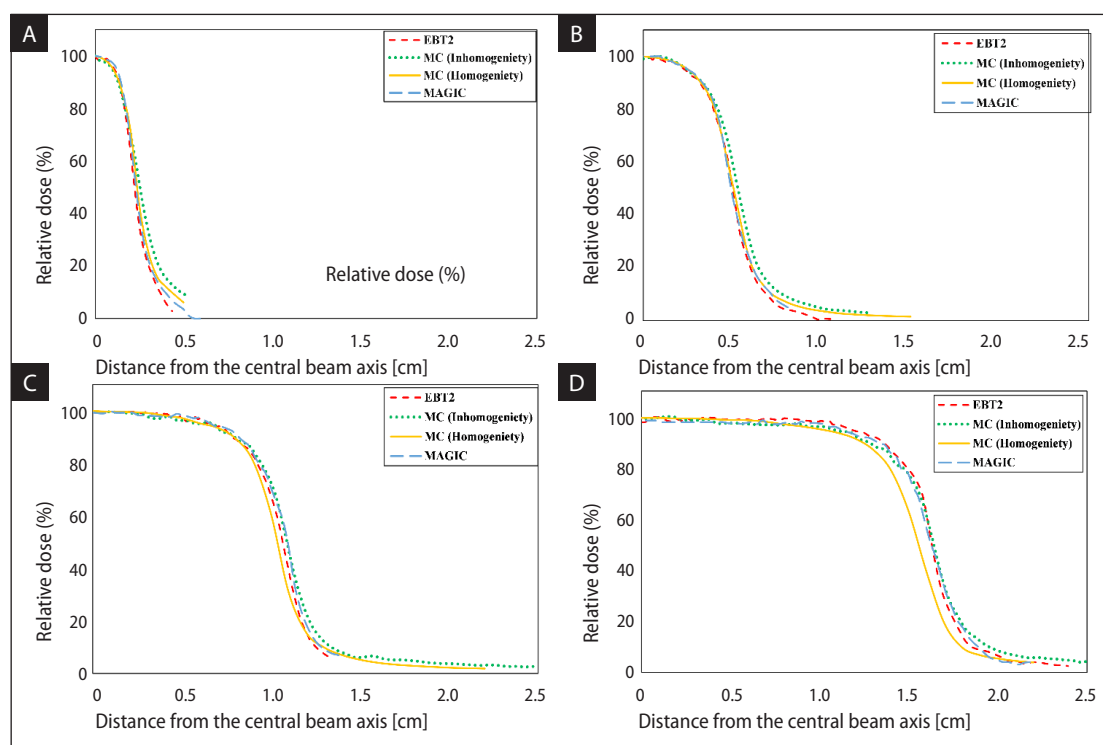


Figure 6. Measured and calculated beam profiles behind bone heterogeneity at 10 cm depth and source to surface distance (SSD) = 100 cm for 5 mm (A), 10 mm (B), 20 mm (C), and 30 mm circular field sizes (D)

Table 1. Measured penumbra widths (80–20%) and (90–10%) behind bone heterogeneity for four circular field sizes 5, 10, 20, and 30 mm at the depth of 10 cm

Cone size [mm]	90–10% [mm]			80–20% [mm]		
	MAGIC	EBT2	MC	MAGIC	EBT2	MC
5	2.7 ± 0.3	2.2 ± 0.2	3.4	1.7 ± 0.2	1.4 ± 0.1	2.1
10	3.9 ± 0.4	3.6 ± 0.2	4.5	2.2 ± 0.3	2.1 ± 0.1	2.4
20	4.6 ± 0.4	4.5 ± 0.2	5.2	2.5 ± 0.2	2.4 ± 0.1	2.6
30	5.5 ± 0.4	5.3 ± 0.2	6.7	3.1 ± 0.3	2.7 ± 0.2	3.4

MAGIC — methacrylic and ascorbic acid in gelatin initiated by copper; MC — Monte Carlo

5, 10, 20, and 30 mm. Penumbra widths (80–20%) were 2.1, 2.2, 2.6, and 3 mm for 5, 10, 20, and 30 mm diameter field sizes, respectively. Also, the values of 3.4, 4.1, 5.1, and 5.5 mm were obtained for penumbra widths (90–10%).

Discussion

The circular small field sizes are mainly used for the treatment of very small tumors such as those seen in the SRS technique to treat brain metastases [24]. In the treatment of small tumors, the small fields made with cone collimators have more benefits than those formed using multi-leaf collimators

due to lower penumbra and transmission [24]. In addition, the cone collimators have high mechanical stability because these collimators do not have moving parts. Therefore, the conical collimators were used in the present work.

MAGIC and EBT2 calibration

As shown in Figure 3, the MAGIC polymer gel exhibits a linear dose-response in the range of 0 to 10 Gy. Considering that the maximum dose delivered to the phantoms in this project was 8 Gy, so it can be concluded that all the curves presented in this study are derived from doses that are in the linear dose-response range of the MAGIC dosimeter.

In addition, a standard deviation of less than 4% in the measured response for all dose levels indicates that the reproducibility of the Magic dosimeter response is acceptable.

Percentage depth dose

The PDD values increased at the initial boundary between soft tissue - bone for all field sizes, as can be seen in figure 5. The dose enhancement in the initial side of a soft tissue/high Z material interface is due to the electron backscattering. The results reported by Wilcox et al. which were performed by EBT film and MC calculation for circular cone sizes of 7.5, 10, 20, and 40 mm, are consistent with the results presented in this study [25]. Also, the doses were decreased at the central axis behind the bone-soft tissue interface in comparison to the measurements for homogeneity were done to show the effect of bone heterogeneity on dosimetric parameters. This is due to the higher beam shielding by bone-equivalent medium compared to soft tissue-equivalent media.

As shown in Figure 5, in the bone heterogeneity region (3 to 6 cm) the PDD values measured by EBT2 films are more than that calculated by Monte Carlo. The main reason is that the electron density of EBT2 films are different than bone [21]. Examination of the dose difference between PDDs measured with EBT2, MAGIC, and Monte Carlo behind bone heterogeneity shows that the MAGIC dosimeter gel is most consistent with the Monte Carlo method compared to EBT2 dosimeter for all field sizes used. This is because the MAGIC dosimeter gel is exactly equivalent to the water, but EBT2 films are different from water in terms of electron density [26]. Also, the maximum differences between MAGIC gel dosimeters and MC calculations decreases as radiation field size increases due to the lateral electronic disequilibrium reduction. Our findings are consistent with the results presented by Parwaie et al. that evaluated the performance of MAGIC polymer gel in homogeneous situation [27].

Beam profile

As shown in Figure 6, beam profiles behind the bone have a lower dose gradient in comparison to the homogeneous condition. This significant reduction in dose gradient can be justified by the wider range of the lateral secondary electrons produced in bone heterogeneity. In addition, as radiation

field size increases the lateral electronic disequilibrium reduces and consequently the slope of the dose profiles increases. Evaluation of all radiation fields showed that the beam profiles obtained with MAGIC gel dosimeter are more consistent with the MC calculations compared to the EBT2 film. This is because the pixel size considered in the MC calculations is approximately equal to the pixels defined in the MRI scanning for the MAGIC.

It can be seen in Table 1 that the penumbra widths (80–20%) and (90–10%) were obtained using MAGIC gel dosimeter and EBT2 film for field sizes of 5, 10, 20, and 30 mm at a depth of 10 cm, and then compared with MC calculated penumbra. According to obtained results, MAGIC and EBT2 dosimeters performed well for the measurement of penumbra width in the presence of high-density heterogeneity due to high spatial resolution. In the measurement of penumbra widths, EBT2 film shows the lowest value compared to MAGIC and MC. This is due to the smaller size of the film pixels than the other dosimeters used in this study. Yarahmadi et al. reported similar results using the EBT2 films for small field sizes (5, 10, 20 and 30 mm diameters) at depth = 5 cm and SSD = 100 [28].

Conclusion

In small field dosimetry, the main uncertainty is Charged particle disequilibrium. The presence of heterogeneous media like bone increased this uncertainty due to beam perturbation. Therefore, an acceptable dosimeter for small photon field dosimetry should have some properties such as having high spatial and dose resolution, being radiological tissue equivalent, and having energy, dose rate, and direction independence. For PDD curves, the MAGIC dosimeter gel is most consistent with the Monte Carlo calculation compared to EBT2 film due to that, MAGIC is more equivalent to water than film. In addition, the beam profiles obtained with MAGIC gel dosimeter were consistent with the MC calculations but for simulation parameters accepted by the user. Although, MAGIC as a polymer gel dosimeter are associated with some challenges such as issues concerning repeatability and their requirement for advanced data processing techniques, it can be candidate as a proper tool to measure the dosimetric parameters in small photon fields, also in the presence bone inhomogeneity, such as those found in the

SRS treatment of small brain tumor of near-spherical shape below the skull bone.

Conflict of interest

The authors declare that they have no known competing financial interests or personal relationships that could have appeared to influence the work reported in this paper.

Funding

Tehran University of Medical Sciences has financially supported the work and this is stated in the acknowledgment section of the article.

References

1. Diwanji TP, Mohindra P, Vyfhuis M, et al. Advances in radiotherapy techniques and delivery for non-small cell lung cancer: benefits of intensity-modulated radiation therapy, proton therapy, and stereotactic body radiation therapy. *Transl Lung Cancer Res.* 2017; 6(2): 131–147, doi: [10.21037/tlcr.2017.04.04](https://doi.org/10.21037/tlcr.2017.04.04), indexed in Pubmed: [28529896](https://pubmed.ncbi.nlm.nih.gov/28529896/).
2. Alfonso R, Andreo P, Capote R, et al. A new formalism for reference dosimetry of small and nonstandard fields. *Med Phys.* 2008; 35(11): 5179–5186, doi: [10.1118/1.3005481](https://doi.org/10.1118/1.3005481), indexed in Pubmed: [19070252](https://pubmed.ncbi.nlm.nih.gov/19070252/).
3. Parwaie W, Refahi S, Ardekani MA, et al. Different Dosimeters/Detectors Used in Small-Field Dosimetry: Pros and Cons. *J Med Signals Sens.* 2018; 8(3): 195–203, doi: [10.4103/jmss.JMSS_3_18](https://doi.org/10.4103/jmss.JMSS_3_18), indexed in Pubmed: [30181968](https://pubmed.ncbi.nlm.nih.gov/30181968/).
4. Stathakis S, Esquivel C, Quino L, et al. Accuracy of the Small Field Dosimetry Using the Acuros XB Dose Calculation Algorithm within and beyond Heterogeneous Media for 6 MV Photon Beams. *Int J Med Phys Clin Engin Radiat Oncol.* 2012; 01(03): 78–87, doi: [10.4236/ijmpcero.2012.13011](https://doi.org/10.4236/ijmpcero.2012.13011).
5. Latifi K, Oliver J, Baker R, et al. Study of 201 non-small cell lung cancer patients given stereotactic ablative radiation therapy shows local control dependence on dose calculation algorithm. *Int J Radiat Oncol Biol Phys.* 2014; 88(5): 1108–1113, doi: [10.1016/j.ijrobp.2013.12.047](https://doi.org/10.1016/j.ijrobp.2013.12.047), indexed in Pubmed: [24529716](https://pubmed.ncbi.nlm.nih.gov/24529716/).
6. Arnfield MR, Otto K, Aroumougame VR, et al. The use of film dosimetry of the penumbra region to improve the accuracy of intensity modulated radiotherapy. *Med Phys.* 2005; 32(1): 12–18, doi: [10.1118/1.1829246](https://doi.org/10.1118/1.1829246), indexed in Pubmed: [15719949](https://pubmed.ncbi.nlm.nih.gov/15719949/).
7. Oliveira L, Calcina CG, Parada M, et al. Ferrous Xylenol Gel measurements for 6 and 10 MV photons in small field sizes. *Brazil J Phys.* 2007; 37(3b): 1141–1146, doi: [10.1590/s0103-97332007000700012](https://doi.org/10.1590/s0103-97332007000700012).
8. Underwood TSA, Thompson J, Bird L, et al. Validation of a prototype DiodeAir for small field dosimetry. *Phys Med Biol.* 2015; 60(7): 2939–2953, doi: [10.1088/0031-9155/60/7/2939](https://doi.org/10.1088/0031-9155/60/7/2939), indexed in Pubmed: [25789823](https://pubmed.ncbi.nlm.nih.gov/25789823/).
9. Burke E, Poppinga D, Schönfeld AA, et al. The practical application of scintillation dosimetry in small-field photon-beam radiotherapy. *Z Med Phys.* 2017; 27(4): 324–333, doi: [10.1016/j.zemedi.2016.11.001](https://doi.org/10.1016/j.zemedi.2016.11.001), indexed in Pubmed: [28342596](https://pubmed.ncbi.nlm.nih.gov/28342596/).
10. Guo PY, Adamovics JA, Oldham M. Characterization of a new radiochromic three-dimensional dosimeter. *Med Phys.* 2006; 33(5): 1338–1345, doi: [10.1118/1.2192888](https://doi.org/10.1118/1.2192888), indexed in Pubmed: [16752569](https://pubmed.ncbi.nlm.nih.gov/16752569/).
11. Calcina CS, de Oliveira LN, de Almeida CE, et al. Dosimetric parameters for small field sizes using Fricke xylenol gel, thermoluminescent and film dosimeters, and an ionization chamber. *Phys Med Biol.* 2007; 52(5): 1431–1439, doi: [10.1088/0031-9155/52/5/014](https://doi.org/10.1088/0031-9155/52/5/014), indexed in Pubmed: [17301463](https://pubmed.ncbi.nlm.nih.gov/17301463/).
12. Pappas E, Maris TG, Zacharopoulou F, et al. Small SRS photon field profile dosimetry performed using a PinPoint air ion chamber, a diamond detector, a novel silicon-diode array (DOSI), and polymer gel dosimetry. Analysis and intercomparison. *Med Phys.* 2008; 35(10): 4640–4648, doi: [10.1118/1.2977829](https://doi.org/10.1118/1.2977829), indexed in Pubmed: [18975710](https://pubmed.ncbi.nlm.nih.gov/18975710/).
13. Kang YN, Choi B, Jang HS, et al. Development of BANG-3?? Polymer Gel Dosimetry System in Small Radiosurgical Fields. *J Korean Phys Soc.* 2011; 59(6): 3422–3427, doi: [10.3938/jkps.59.3422](https://doi.org/10.3938/jkps.59.3422).
14. Shih TY, Wu J, Shih CT, et al. Small-Field Measurements of 3D Polymer Gel Dosimeters through Optical Computed Tomography. *PLoS One.* 2016; 11(3): e0151300, doi: [10.1371/journal.pone.0151300](https://doi.org/10.1371/journal.pone.0151300), indexed in Pubmed: [26974434](https://pubmed.ncbi.nlm.nih.gov/26974434/).
15. Low DA, Parikh P, Dempsey JF, et al. Ionization chamber volume averaging effects in dynamic intensity modulated radiation therapy beams. *Med Phys.* 2003; 30(7): 1706–1711, doi: [10.1118/1.1582558](https://doi.org/10.1118/1.1582558), indexed in Pubmed: [12906187](https://pubmed.ncbi.nlm.nih.gov/12906187/).
16. Laub WU, Kaulich TW, Nüsslin F. A diamond detector in the dosimetry of high-energy electron and photon beams. *Phys Med Biol.* 1999; 44(9): 2183–2192, doi: [10.1088/0031-9155/44/9/306](https://doi.org/10.1088/0031-9155/44/9/306), indexed in Pubmed: [10495113](https://pubmed.ncbi.nlm.nih.gov/10495113/).
17. Rustgi SN, Frye DM. Dosimetric characterization of radiosurgical beams with a diamond detector. *Med Phys.* 1995; 22(12): 2117–2121, doi: [10.1118/1.597655](https://doi.org/10.1118/1.597655), indexed in Pubmed: [8746721](https://pubmed.ncbi.nlm.nih.gov/8746721/).
18. Allahverdi M, Sarkhosh M, Aghili M, et al. Evaluation of treatment planning system of brachytherapy according to dose to the rectum delivered. *Radiat Prot Dosimetry.* 2012; 150(3): 312–315, doi: [10.1093/rpd/ncr415](https://doi.org/10.1093/rpd/ncr415), indexed in Pubmed: [22128355](https://pubmed.ncbi.nlm.nih.gov/22128355/).
19. Wong CJ, Ackerly T, He C, et al. Small field size dose-profile measurements using gel dosimeters, gafchromic films and micro-thermoluminescent dosimeters. *Radiat Measurements.* 2009; 44(3): 249–256, doi: [10.1016/j.radmeas.2009.03.012](https://doi.org/10.1016/j.radmeas.2009.03.012).
20. Fong PM, Keil DC, Does MD, et al. Polymer gels for magnetic resonance imaging of radiation dose distributions at normal room atmosphere. *Phys Med Biol.* 2001; 46(12): 3105–3113, doi: [10.1088/0031-9155/46/12/303](https://doi.org/10.1088/0031-9155/46/12/303), indexed in Pubmed: [11768494](https://pubmed.ncbi.nlm.nih.gov/11768494/).
21. Mohammad A, Nedaie H, YarAhmadi M, et al. Dosimetric Evaluation of Heterogeneities in Small Circular Fields of 6 MV Photon Beams with EBT2 and EDR2 Films: Comparison with Monte Carlo Calculation. *J Modern Phys.* 2014; 05(16): 1608–1616, doi: [10.4236/jmp.2014.516162](https://doi.org/10.4236/jmp.2014.516162).
22. Palmans H, Andreo P, Huq MS, et al. Dosimetry of small static fields used in external photon beam radiotherapy: Summary of TRS-483, the IAEA-AAPM international Code of Practice for reference and relative dose determination. *Med Phys.* 2018; 45(11): e1123–e1145, doi: [10.1002/mp.13208](https://doi.org/10.1002/mp.13208), indexed in Pubmed: [30247757](https://pubmed.ncbi.nlm.nih.gov/30247757/).

23. Sevcik A, Adliene D, Laurikaitiene J, et al. Low energy deposition patterns in irradiated phantom with metal artefacts inside: a comparison between FLUKA Monte Carlo simulation and GafChromic EBT2 film measurements. *Nuclear Instruments and Methods in Physics Research Section B: Beam Interactions with Materials and Atoms*. 2020; 478: 142–149, doi: [10.1016/j.nimb.2020.06.003](https://doi.org/10.1016/j.nimb.2020.06.003).
24. Hermida-López M, Sánchez-Artuñedo D, Rodríguez M, et al. Monte Carlo simulation of conical collimators for stereotactic radiosurgery with a 6 MV flattening-filter-free photon beam. *Med Phys*. 2021; 48(6): 3160–3171, doi: [10.1002/mp.14837](https://doi.org/10.1002/mp.14837), indexed in Pubmed: [33715167](https://pubmed.ncbi.nlm.nih.gov/33715167/).
25. Wilcox EE, Daskalov GM. Accuracy of dose measurements and calculations within and beyond heterogeneous tissues for 6 MV photon fields smaller than 4 cm produced by Cyberknife. *Med Phys*. 2008; 35(6): 2259–2266, doi: [10.1118/1.2912179](https://doi.org/10.1118/1.2912179), indexed in Pubmed: [18649456](https://pubmed.ncbi.nlm.nih.gov/18649456/).
26. Ramirez JLV, Chen F, Nicolucci P, et al. Dosimetry of small radiation field in inhomogeneous medium using alanine/EPR minidosimeters and PENELOPE Monte Carlo simulation. *Radiat Measurements*. 2011; 46(9): 941–944, doi: [10.1016/j.radmeas.2011.06.008](https://doi.org/10.1016/j.radmeas.2011.06.008).
27. Parwaie W, Yarahmadi M, Nedaie HA, et al. Evaluation of MRI-based MAGIC polymer gel dosimeter in small photon fields. *Int J Radiat Res*. 2016; 14(1): 59–65, doi: [10.18869/acadpub.ijrr.14.1.59](https://doi.org/10.18869/acadpub.ijrr.14.1.59).
28. Yarahmadi M, Nedaie H, Allahverdi M, et al. Small photon field dosimetry using EBT2 Gafchromic film and Monte Carlo simulation. *Int J Radiat Res*. 2013; 11(4): 215.